

Probing the Structure of the Pomeron

John Ellis

Theoretical Physics Division,
CERN,
1211 Geneva 23,
Switzerland

Graham G. Ross and Jenny Williams

Dept. of Physics,
Theoretical Physics,
1 Keble Rd.,
Oxford OX1 3NP

June 18, 2021

Abstract

We suggest that the pseudo-rapidity cut dependence of diffractive deep-inelastic scattering events at HERA may provide a sensitive test of models of diffraction. A comparison with the experimental cross section shows that the Donnachie-Landshoff model and a simple two-gluon exchange model of the pomeron model are disfavoured. However a model with a direct coupling of the pomeron to quarks is viable for a harder quark–pomeron form factor, as is a model based on the leading-twist operator contribution. We also consider a direct-coupling scalar pomeron model. We comment on the implications of these results for the determination of the partonic structure of the pomeron.

1 Introduction

Pomeron exchange is familiar as a description of total hadron-hadron cross sections that rise slowly with increasing energy [1]. It should also play a major role in the diffractive events that have been observed in electron-proton deep-inelastic scattering (DIS) at HERA, where the diffractive system may be isolated by requiring that it be separated from the proton direction by a large gap in pseudo-rapidity [2, 3]. Large pseudo-rapidity gaps imply

the exchange of a colourless state between the proton and the virtual photon, and the leading contribution to these events is often interpreted as due to pomeron exchange [1]. These pseudo-rapidity gap events can be viewed as the proton emitting a pomeron which then undergoes deep-inelastic scattering. Ingelman and Schlein [4] suggested treating the pomeron as an hadronic particle. In this picture, one may consider diffractive DIS to be a probe of the partonic structure of the pomeron. This is a *resolved-coupling* scheme, as the high-energy photon sees the constituent partons in the pomeron. That is, the quarks and gluons to which the pomeron couples are considered to be constituents of the pomeron, and hence are necessarily close to mass shell. The basic diagram which illustrates this scheme is shown in Fig. 1, where one may imagine that the photon is probing the quark structure of the pomeron. Higher-order processes include gluon bremsstrahlung, as shown in Fig. 2a, and boson-gluon fusion, as shown in Fig. 2b, in which the photon interacts with the gluonic structure of the pomeron. The resolved-coupling interpretation does not include direct couplings between the pomeron and off-shell partons.

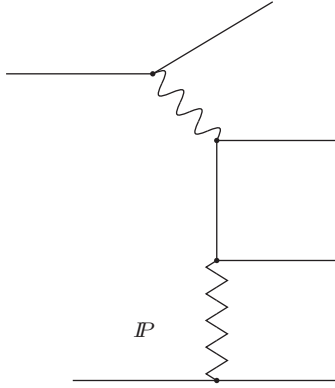


Figure 1: *Diffractive DIS via pomeron exchange.*

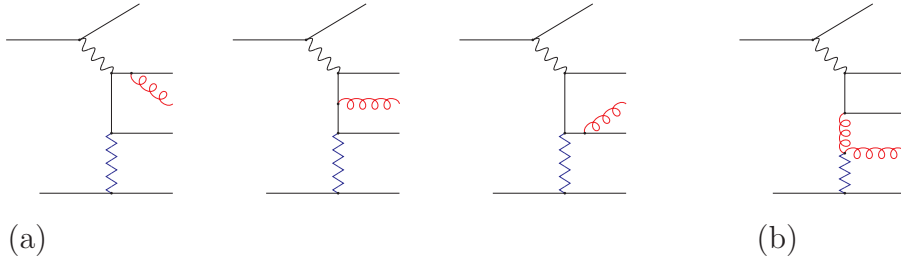


Figure 2: *Higher-order QCD corrections to diffractive scattering via pomeron exchange, due to (a) gluon bremsstrahlung and (b) boson-gluon fusion diagrams.*

In this hadronic picture of the pomeron, one can factorize the diffractive scattering cross

section into a sum over the product of the probability to find a parton with momentum fraction β in the pomeron and the cross section for parton-photon hard scattering. In analogy with standard DIS, one can define a diffractive structure function for these processes in terms of the diffractive cross section,

$$\frac{d^3\sigma^{\text{diff}}}{d\beta dQ^2 dx_P} = \frac{2\pi\alpha^2}{\beta Q^4} [(1 + (1 - y)^2) F_2^{D(3)}(\beta, Q^2, x_P) - y^2 F_L(\beta, Q^2, x_P)], \quad (1)$$

where for $y \lesssim 0.4$ the longitudinal term can be neglected [5]. According to this picture for leading pomeron exchange, the diffractive structure function can be written in terms of a *pomeron structure function*, $F_2^P(\beta, Q^2)$,

$$F_2^{D(3)}(\beta, Q^2, x_P) = f^P(x_P) F_2^P(\beta, Q^2). \quad (2)$$

Here f^P describes the pomeron flux in the proton, β plays the role of the Bjorken x variable in DIS, and F^P is interpreted as the structure function of the pomeron. Experimental results from HERA are consistent with this factorization for a wide range of parameters [6]. Factorization breaking can be interpreted as being due to sub-leading Reggeon ($\rho, \omega \dots$) exchanges [8].

One consequence of a strong pseudo-rapidity cut selection [7] is that it tends to force the parton far off-shell, introducing a further possible source of factorization breaking into the diffractive structure function. This is because the experimentally extracted diffractive structure function is obtained by integrating the differential cross section over the kinematically accessible phase space. As shown in Appendix A.1, the lower limit $\theta_{\text{min}}^{\text{cms}}$ of the angular integral is a sensitive function of the kinematic parameters Q^2 , β and x_P . Therefore, as we discuss in Sect. 5, a further, unfactorizable, x_P -dependence is introduced into the diffractive structure function through the lower limit of the phase-space integral. As a result, one would not expect a diffractive structure function selected by making a large pseudo-rapidity cut, requiring large virtuality, to be factorizable into a pomeron flux factor and an x_P -independent pomeron “structure function”, even though the full structure function (integrated over the whole phase space) may be factorizable.

As discussed in [7], events with a strong pseudo-rapidity cut offer a way of discriminating between models with direct and resolved couplings. Here we sharpen the previous analysis of the kinematical constraints implied by pseudo-rapidity gap cuts, and discuss how they may offer a sensitive discriminator between various models proposed to describe deep-inelastic diffractive scattering. We present a comparison with experiment of the pseudo-rapidity dependence for five models. The first is the Donnachie-Landshoff (D-L) model [9], which employs a vector-like direct coupling of the Pomeron to quarks, assuming a soft form factor. The second is a modification of this scheme suggested by two of the authors (E-R) [7], which invokes a harder form factor. The third model assumes a scalar direct coupling to quarks [10]. The fourth model uses two-gluon exchange to model the Pomeron [11], and the final model assumes that the pseudo-rapidity gap events can be described by the operator-product expansion (OPE), with dominance by the leading-twist operator. Finally we discuss the implications of our analysis for the prospects of probing the parton structure of the Pomeron.

In Sect. 2 we describe the kinematics of diffractive deep-inelastic electron-proton scattering. Following this, in Sect. 3 we discuss the parton virtuality constraints implied by strong pseudo-rapidity cuts, the derivations of which are given in Appendices A.1 and A.2. In Sect. 4 we discuss our selection of the various models that have been proposed to describe diffractive deep-inelastic scattering. In Sect. 5 we compare the predictions of these models for the pseudo-rapidity gap dependence with experiment. Finally, we look at the consequences of large virtuality constraints for previous analyses and suggest in Sect. 6 further experimental investigations to test the ideas presented here. A summary and conclusions are presented in Sect. 7.

2 Kinematics of Diffractive Deep-Inelastic Scattering

In the HERA electron-proton experiments, 820 GeV protons collide with 27.5 GeV electrons or positrons. This corresponds to a centre-of-mass (CMS) energy $\sqrt{s} \sim 300$ GeV, and allows access to a wider range of Q^2 and Bjorken x than has previously been possible. In the HERA lab frame, the positive z axis is defined to be in the forward proton direction and the origin is at the interaction vertex. We consider diffractive deep-inelastic $e - P$ scattering,

$$e(p_e) + P(P) \rightarrow e(p'_e) + P(P') + X(X), \quad (3)$$

where the momenta of the particles are shown in brackets. The hadronic system X is assumed to be separated from the forward proton direction by a large pseudo-rapidity gap. We assume that the proton (or low-mass excited state) escapes undetected down the beam-pipe or is detected far downstream [6]. The contribution from proton dissociation is limited by acceptance cuts: if M_Y is the mass of the proton remnant, then for H1 $M_Y \lesssim 1.6$ GeV, and for ZEUS $M_Y \lesssim 4$ GeV. One may consider that the interaction proceeds by virtual photon–pomeron deep-inelastic scattering,

$$\gamma^*(q) + \mathbb{P}(P_P) \rightarrow X(X), \quad (4)$$

where $P_P = P - P'$.

We use the usual kinematic variables of deep-inelastic scattering:

$$Q^2 = -q^2, \quad x = \frac{Q^2}{2P \cdot q}, \quad \text{and} \quad y = \frac{Q^2}{xs}, \quad (5)$$

where Q^2 is the negative 4-momentum squared of the virtual photon and x is the Bjorken scaling variable. We also define W^2 , the mass squared of the total hadronic system (X + outgoing proton), by

$$W^2 = (P + q)^2. \quad (6)$$

Additionally, for diffractive scattering we define

$$t_P = (P - P')^2, \quad x_P = \frac{(P - P') \cdot q}{P \cdot q} \approx \frac{Q^2 + M_X^2}{Q^2 + W^2}, \quad \text{and} \quad \beta = \frac{Q^2}{2(P - P') \cdot q} \approx \frac{Q^2}{Q^2 + M_X^2}, \quad (7)$$

where t_P is the momentum transfer at the proton vertex and is constrained by experimental cuts to be small ($|t_P| \lesssim 1 \text{ GeV}^2$), x_P is the fraction of longitudinal momentum of the proton carried by the pomeron,¹ and $x = \beta x_P$. The mass squared of the diffractive system X is M_X^2 , and the proton mass is neglected in this analysis. In the lowest-order diagram shown in Fig. 1, β is interpreted as the fraction of the pomeron momentum carried by the struck quark, whereas in the three-jet diagrams of Fig. 2, β is the fraction of pomeron momentum in the exchanged parton which couples to the pomeron.

The *pseudo-rapidity* η of an outgoing particle is defined in the laboratory frame in terms of its polar angle with respect to the proton direction:

$$\eta = -\ln \tan \left(\frac{\theta_{\text{lab}}}{2} \right). \quad (8)$$

In the Ingelman-Schlein picture [4], diffractive DIS corresponds to probing the partonic structure of the pomeron. For example, the leading contribution to diffractive scattering is the dijet diagram of Fig. 1, in which the high-energy photon sees the quark content of the pomeron. Higher-order processes include the gluon bremsstrahlung of Fig. 2a and the boson-gluon fusion of Fig. 2b, in which the photon interacts with the gluonic structure of the pomeron.

For the process of Fig. 1, we introduce a further invariant, the four-momentum squared of the struck quark, k^2 . In the $\gamma^* - \mathbb{P}$ CMS system, the virtuality of this quark can be expressed in terms of other invariants, and the polar angle with respect to the $\gamma^* \mathbb{P}$ axis, by

$$k^2 = -\frac{Q^2 + M_X^2}{2}(1 - \cos \theta_{\text{cms}}). \quad (9)$$

A similar expression can be formed for interactions, such as those of Fig. 2, where more than two final-state partons are produced.

3 Virtuality Constraints from Experimental Cuts

In a typical measurement with a pseudo-rapidity cut, diffractive events are selected by requiring there to be no activity observed above a low-energy threshold (400 MeV) in a large pseudo-rapidity interval about the forward proton direction. Thus only events with pseudo-rapidity less than some cut, η_{max} , are accepted. On the other hand, for an hadronic interpretation of the pomeron, we would require the quarks coupling to the pomeron to be near mass shell ($|k^2| \lesssim \Lambda_{\text{QCD}}^2$). It has been observed that the strong pseudo-rapidity cuts imposed in early H1 and ZEUS analyses [2,3] restricted the phase space available for diffractive scattering, and selected only events in which the struck quark of Fig. 1 was forced to be far off mass

¹To a good approximation for very small t_P , the pomeron is emitted in the forward proton direction.

shell for a wide region of parameter space [7]. This means that the selection cuts rejected all events corresponding to the process of Fig. 1 for a wide range of parameters.

To demonstrate this, note that a cut in pseudo-rapidity corresponds to a lower bound on θ_{cms} , which translates to a lower bound, k_{min}^2 , on the struck quark virtuality. As was shown previously [7], for strong pseudo-rapidity cuts η_{max} , and for a wide range of β , Q^2 and $x_{\mathcal{P}}$, the struck quark in the diagram of Fig. 1 is forced to be far off shell, i.e., $-k_{\text{min}}^2 > 1 \text{ GeV}^2$.² The result is a relation between η_{max} and k_{min}^2 in terms of the laboratory energies of the electron and proton and the kinematic variables defined in the previous section. The details of this calculation are given in Appendix A.1. Apart from correcting a small error, the main difference between the new and old calculations [7] is due to the elimination of a small-angle approximation made in the original analysis.

The virtuality constraints following from the pseudo-rapidity cuts used in early ZEUS analyses are given in Table 1, following [7]. Tabulated diffractive structure function data for a pseudo-rapidity cut of $\eta_{\text{max}} = 1.8$ and much stronger virtuality constraints appear in [12]. The kinematic parameters of these data and the corresponding virtuality constraints, k_{min}^2 , are shown in Table 2. This clearly demonstrates that, in a resolved-coupling picture, events due to the process of Fig. 1 do not contribute to large pseudo-rapidity gap diffractive DIS in a wide region of parameter space.

Q^2 GeV ²	β	$x_{\mathcal{P}}$	$-k_{\text{min}}^2 \text{ GeV}^2$ ($\eta_{\text{max}} = 1.5$)	$-k_{\text{min}}^2 \text{ GeV}^2$ ($\eta_{\text{max}} = 2.5$)	$-k_{\text{min old}}^2 \text{ GeV}^2$ ($\eta_{\text{max}} = 1.5$)	$-k_{\text{min old}}^2 \text{ GeV}^2$ ($\eta_{\text{max}} = 2.5$)
10	0.175	.0032	2.5	0.39	3.1	0.4
		.0050	5.1	0.89	7.5	1.0
	0.375	.0020	0.7	0.11	0.9	0.12
		.0032	1.5	0.27	2.3	0.3
	0.65	.0013	0.2	0.03	0.2	0.03
		.0020	0.3	0.06	0.5	0.07
28	0.175	.0050	6.2	0.95	7.5	1.0
		.0079	13.3	2.26	18.7	2.5
	0.375	.0020	0.8	0.12	0.9	0.1
		.0079	7.4	1.51	14.2	1.9
	0.65	.0020	0.4	0.06	0.5	0.07
		.0050	1.7	0.33	3.2	0.4
63	0.375	.0050	4.5	0.71	5.7	0.8
		.0079	9.4	1.66	14.2	1.9
	0.65	.0032	1.0	0.16	1.3	0.2
		.0079	4.1	0.83	8.0	1.1

Table 1: *Constraints on the virtuality of the struck quark from the pseudo-rapidity cuts used in early ZEUS experiments [3]. In this Table, $k_{\text{min old}}^2$ corresponds to the results published in [7], and k_{min}^2 are the revised virtuality constraints with small corrections due principally to the elimination of the small-angle approximation used in [7].*

²We note that the experimental cuts are made at the hadron level, and that our calculations are at parton level. The corresponding estimate of η_{max} at the parton level uses a conservative estimate of the hadronization radius [3], namely, it assumes that hadronization radius spans approximately half a unit in pseudo-rapidity. We have tested the robustness of our calculations by also considering the extreme cases where the hadronizing parton is at either edge of the resulting jet, finding that a large lower bound, $-k_{\text{min}}^2 \gtrsim 1 \text{ GeV}^2$, on the exchanged quark virtuality remains.

$Q^2 \text{ GeV}^2$	β	$x_{\mathbb{P}}$	$-k_{\min}^2 \text{ GeV}^2$	$-k_{\max}^2 \text{ GeV}^2$	$\theta_{\min}^{\text{cms}}$
8.5	0.065	0.00365	2.3	130	15
		0.00649	6.7	130	26
12	0.065	0.00649	6.9	180	22
		0.01154	19	180	37
		0.02052	44	180	59
		0.03648	82	180	84
	0.175	0.00429	2.5	69	22
		0.00762	6.4	69	36
		0.01355	14	69	54
		0.02410	26	69	75
	0.375	0.00356	1.1	32	22
		0.00632	2.7	32	34
		0.01125	5.5	32	49
25	0.65	0.00649	1.2	18	29
		0.01154	21	390	27
		0.02052	55	390	44
		0.03648	120	390	68
	0.175	0.06488	200	390	93
		0.00429	2.7	140	16
		0.00762	7.4	140	26
		0.01355	18	140	42
	0.375	0.02410	38	140	62
		0.04285	62	140	83
		0.00356	1.3	67	16
		0.00632	3.3	67	26
50	0.65	0.01125	7.5	67	39
		0.02000	14	67	55
		0.00649	1.5	38	23
		0.01154	3.1	38	33
	0.175	0.00762	8.2	290	20
		0.01355	22	290	32
		0.02410	51	290	50
		0.04285	95	290	71
	0.375	0.07620	140	290	90
		0.00356	1.4	130	12
		0.00632	3.8	130	19
		0.01125	9.4	130	31
	0.65	0.02000	20	130	46
		0.03556	35	130	62
		0.00649	1.9	77	18
		0.01154	4.2	77	27
		0.02052	7.9	77	37

Table 2: *Virtuality constraints for diffractive scattering as a function of Q^2 , β , and $x_{\mathbb{P}}$ for the parameter range measured in [12]. The constraints correspond to the pseudo-rapidity cut of $\eta_{\max}^{\text{exp}} = 1.8$ which was used for data selection. Also shown is k_{\max}^2 , which is the maximum possible virtuality of the exchanged quark.*

We have extended the original calculation to include large pseudo-rapidity gap diffractive production of three or more partons, which we term “multi-jet” production, due, e.g., to the diagrams of Fig. 2. Here we consider the virtuality of the exchanged parton coupling to the pomeron. In the boson-gluon fusion case, for example, we are concerned with the virtuality of the exchanged gluon. We find that the constraint on the virtuality of this parton is slightly weaker than in the dijet case, but still find that the large pseudo-rapidity gap selection cuts rule out resolved-coupling contributions from these diagrams for most of the data points corresponding to Table 2. The details of this calculation are given in Appendix A.2.

4 Implications and Models of the Pseudo-Rapidity Gap Dependence

The result of this analysis has been to show that, for a subclass of the deep-inelastic diffractive events, the relevant colour-singlet exchange process, pomeron exchange, must involve a direct coupling to off-shell partons involved in the hard-scattering process. This is a significant result because, at first sight, such a component is *not* the usual parton contribution to inclusive deep-inelastic scattering processes that is often used to interpret the data in terms of a “pomeron” structure function. In particular, our results show that the graphs involving t -channel colour non-singlet exchange in the hard-scattering sub-process should not be included in describing the deep-inelastic exclusive processes involving strong pseudo-rapidity cuts. However, pseudo-rapidity cut events exhibit scaling and form a significant part of the inclusive deep-inelastic scattering events which *are* governed by the operator product expansion (OPE). The latter ascribes the dominant scaling contribution in deep-inelastic inclusive scattering to just the colour exchange graphs which we argue must be absent from the exclusive strong pseudo-rapidity cut events. These leading-twist graphs have also been shown directly to dominate exclusive diffractive processes, using an expansion in non-local operators [13, 14]. However, it is not clear that this analysis applies to the more exclusive pseudo-rapidity gap events of interest here.

There are two possibilities for reconciling our results on the importance of colour-singlet exchange with this expected need for colour-exchange processes. The first arises because the events being studied at HERA are at extremely small x_{Bjorken} , in a region where the OPE, which is reliable when there is only one large variable, may break down because Q^2 and ν , although both large, are not of the same order. We know that such a breakdown must occur in the transition to forward scattering, which is governed by $t = 0$ non-perturbative Regge-exchange processes. If naive perturbation theory does fail, one is forced to adopt a more phenomenological approach to the diffractive scattering of the struck quarks off the proton target. Donnachie and Landshoff have suggested that diffractive quark-proton scattering occurs through a direct coupling of a colourless pomeron to the quark [9]. In analogy with their successful analysis of hadron-hadron diffractive scattering [1], they assume that this process proceeds via vector exchange with a form factor at the quark vertex to describe the dependence on the quark virtuality. The latter is required to avoid power-law violations of the observed scaling in deep-inelastic diffractive processes. In a similar spirit, Vermaseren *et al.* (VBLY) [10] consider a scalar effective exchange interaction to describe the same process.

A second possible way to resolve the apparent discrepancy between the observation of scaling in the large pseudo-rapidity gap events and the OPE does not involve abandoning the OPE for the values of x_{Bjorken} probed at HERA. This possibility is motivated by the observation that the x_{Bjorken} and Q^2 dependence of inclusive deep-inelastic scattering is well fitted by a continuation of the usual DGLAP analysis to small x_{Bjorken} . In this case, the large pseudo-rapidity gap events, while not being directly described by the OPE analysis, because of their exclusive nature, must obey the constraints on the inclusive cross section of which they are a part. In order to make connection with the usual QCD description of deep-inelastic scattering, it is necessary to couple the pomeron to near-mass-shell quarks and/or gluons. Given the discussion above, this must be via colour-singlet exchange due to a diagram such as that in Fig. 3. How does such a diagram fit into the OPE framework? At first sight, it would seem that Fig. 3 corresponds to a higher-twist operator contribution, because we cannot form a twist-two operator from the four physical gluons involved in the square of the scattering amplitude. This would mean that the associated structure function should be suppressed relative to the twist-two contribution by a factor $\mathcal{O}(\Lambda^2/Q^2)$, where Λ is a hadronic scale, i.e., the associated structure function should not scale, in disagreement with the measured structure function. However, the identification of the diagrams of Fig. 3 with higher-twist operators is not correct if the right-hand gluon leaves the quark near its mass shell. In this case, the hard-scattering process is that involving the left-hand gluon only, and the diagram should be identified with the leading twist-two gluon operator. The subsequent soft-scattering process involving the right-hand gluon should properly be included in the soft dressing that is implicitly present in any description of deep-inelastic scattering in order to obtain a final state involving colourless hadrons. The soft parton emission processes discussed in Appendix A.2 also contribute to this dressing. In the fully inclusive scattering case the sum of such dressing forms a complete sum and thus drops out of the calculation of the total cross section.

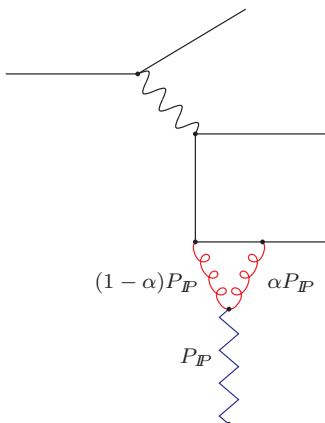


Figure 3: *Two-gluon contribution to the pomeron form factor.*

In what follows we shall discuss both the above possibilities, and try to determine which

best describes the pseudo-rapidity gap events. As mentioned above, the direct coupling has been variously described in terms of a vector-like coupling to quarks [7, 9], and also in terms of a model in which the pomeron has a point-like scalar coupling to quarks and gluons³ [10]. The vector-like exchange model is motivated by the success of the Donnachie-Landshoff (D-L) description of diffractive proton-proton and proton-antiproton scattering in terms of vector exchange with Wu-Yang couplings to the nucleon. They suggested that Pomeron exchange should be treated as a C -even vector-exchange process with γ_μ couplings to the incident proton and the quark involved in the deep-inelastic process as shown in Fig. 1⁴. The expected Regge behaviour at large centre-of-mass energies is put in by hand. In order to generate a cross section consistent with the observed scaling, they introduced a *form factor* at the quark vertex of the form

$$f(k^2) = \frac{\Lambda^2}{\Lambda^2 - k^2}, \quad (10)$$

where k is the four momentum of the struck quark ($0 \leq |k^2| \leq Q^2/\beta$) in Fig. 1 and $\Lambda = \mathcal{O}(\Lambda_{\text{QCD}})$. This choice of form factor allows the pomeron to couple to off-shell partons, but results in the dominant contribution to the diffractive cross section coming from small k^2 . This means that the model is very sensitive to strong pseudo-rapidity cuts, and it was argued in [7] that the cross section falls off too rapidly with decreasing pseudo-rapidity to be able to explain the number of events seen in the large pseudo-rapidity gap sample.

A variant of the model was considered in [7] (E-R), where a harder form factor was chosen:

$$f(k^2) = \sqrt{\frac{\Lambda^2}{\Lambda^2 - k^2}}, \quad (11)$$

which leads to a prediction of additional logarithmic scaling violations. Possible motivation for such a form comes from underlying QCD diagrams, as shown in Fig. 3. As compared to the diagram of Fig. 1, we have an extra fermion propagator between the two gluon lines, leading to the harder form factor of (11). Such a choice is consistent with measurements [8] of the diffractive structure function $F_2^{D(3)}$. Since this form factor falls off more slowly with k^2 than that of (10), the contribution from higher virtuality states is enhanced. In fact, using (11), one finds a uniform contribution from all virtualities up to the maximum [7].

The third direct coupling model assumes effective scalar exchange as treated in [10]. In this case, no form factor is needed, as the cross section scales without it.

An alternative and possibly complementary approach to modelling the direct (colour-singlet) coupling of the pomeron to the quarks is via the colour singlet-component of multi-gluon exchange diagrams, in which the gluons couple to the quarks involved in the hard-scattering process. The simplest graphs are the two-gluon exchange processes shown in Fig. 4 [15]. Clearly, this can only be an approximation to pomeron exchange, but it does capture some of the important features, and does contribute to the large pseudo-rapidity gap

³Here we consider only the dijet component of the VBL model.

⁴Note that the soft parton (gluon) emission processes discussed in Appendix A.2 do *not* fit into this description, because they correspond to the scattering of a C -odd gluon (leading-twist) on the struck quark.

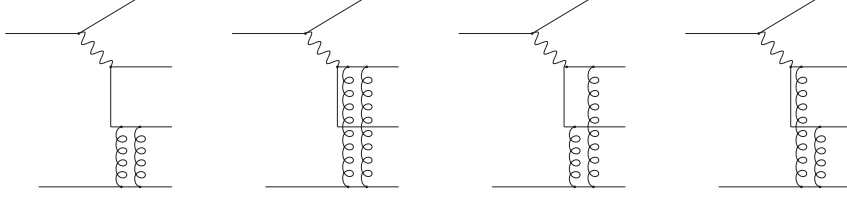


Figure 4: *Two-gluon exchange graphs used to model pomeron exchange.*

events. As is clear from our discussion above, the direct coupling models *à la* Donnachie-Landshoff contain a component of two-gluon exchange, but the latter has the advantage of allowing for a non-local coupling of the pomeron to both the struck quarks.

Of course these two interpretations need not be distinct, in the sense that the two-gluon contribution of Fig. 3 to the pomeron may be interpreted as a direct coupling of the pomeron to quarks with a form factor. In this case, the first two diagrams of Fig. 4 may be interpreted as part of the direct contribution. However, gauge invariance then requires that the remaining two diagrams of Fig. 4 be included, and these cannot be interpreted as a direct coupling of the pomeron to a single quark. However, due to the extra hard propagator involved in these terms, their contribution occurs only at higher twist. A consequence of this is that, beyond leading twist, the direct coupling models at best apply in a specific gauge, namely the gauge in which the contributions of the diagrams of the type corresponding to the third and fourth diagrams of Fig. 4 are minimized [11, 17].

On the other hand, as we have also discussed, a component of these multi-gluon exchange graphs should be identified with the leading-twist exchange. In the two-gluon case, the leading-twist contribution corresponds to the imaginary part of the amplitude which is indeed thought to dominate diffractive scattering. In this part, the intermediate quark coupling to the right-hand gluon is on shell, and this is the component that we argued has a leading-twist component. For the case of more than two gluons, the projection onto the imaginary part is not sufficient to avoid large quark propagators appearing. The phase space associated with the relevant leading-twist configuration is quite small for the large pseudo-rapidity gap events. To see this, note that the pseudo-rapidity cut requires $2k \cdot p > -k_{\min}^2$. Thus, to keep the quark propagators to the right of the left-hand gluon close to mass shell, the fraction, $1-\alpha$, of the pomeron momentum carried by the left-hand gluon must be large, $\alpha \leq \Lambda^2/2k \cdot p \leq \Lambda^2/(-k_{\min}^2)$, corresponding to a small phase space factor for such effects. This suggests that either the two-gluon graph dominates, in which case this constraint follows for the dominant imaginary part, or there are a large number of such soft gluons associated with the colour field of the proton remnant, so that the sum over the “dressing” gluons compensates for the small phase space available. The latter picture has been proposed by Buchmüller and Hebecker [18]. In this picture, the primary hard scattering is due to the usual one-gluon exchange, followed by random soft dressing in the field of the proton remnant. As discussed above, this picture is entirely consistent with the OPE or related [13, 14] expansions, and corresponds to keeping the leading-twist contribution. This leading-twist interpretation of

the pseudo-rapidity gap events does not fit easily with the “particle” interpretation of the Pomeron as a bound state with a significant two-gluon component, because there is no obvious way that the soft gluon dressing should build up a pole in the t channel corresponding to the Pomeron singularity.

Note again that the fact that the pseudo-rapidity cut requires colour-singlet exchange in the t -channel, combined with the leading-twist constraint, requires that a single gluon carries the bulk of the pomeron momentum. This is true also of the soft-parton emission processes which are discussed in Appendix A.2, and which *are* included in the leading-twist contribution. The requirement that a single parton carries most of the Pomeron momentum is a purely kinematical constraint, and does not imply that the same is true for the full partonic structure of the Pomeron. However, in the leading-twist model, the fact that the event rate requiring a stringent pseudo-rapidity gap is comparable to the event rate without this cut does suggest such a component is a significant part of the partonic structure.

5 Pseudo-rapidity Gap Tests

We turn now to the comparison of these models with experiment. The data we use are the large pseudo-rapidity cut events described above, and Table 2 shows the parameters of the data set chosen, where the experimental cut on pseudo-rapidity is $\eta_{\max} = 1.8$. From this Table, we can see that the virtuality constraints rule out any contribution from dijet production. Appendix A.2 shows that the multi-jet contribution has a lower limit on the virtuality of the exchanged parton coupled to the pomeron, so, as we can see from Table 2, most of the data sample corresponds to regions where multi-jet events are also not selected.

It is clearly of interest to try to use these data to discriminate between the various models suggested to describe deep-inelastic diffractive scattering. Here we take a step in this direction by computing the dependence of the deep-inelastic diffractive scattering cross section and diffractive and pomeron structure functions on the pseudo-rapidity cut for several of the models discussed above.

We first compute this dependence for the case in which pomeron exchange is modelled by a vector $C = +1$ exchange, with a form factor at the quark vertex as discussed above. We also consider the VBLY model, in which the pomeron is assumed to have a scalar coupling to quarks. The second class of model we consider is the leading-twist Buchmüller-Hebecker type model, in which a single gluon is responsible for the hard scattering. In this case, the pseudo-rapidity gap dependence is due to single-gluon exchange as in exclusive deep-inelastic scattering. The second (and possibly further) gluon is then simply there to provide soft dressing to produce colour-singlet final states, and is assumed not to affect the pseudo-rapidity cut dependence. Finally, we consider the case in which the pomeron is replaced by two gluons, following the calculation of Diehl [11]. We will also comment at the end on the related two-gluon model of [19].

We start with the direct-coupling models with vector-like coupling. In Fig. 5 we show the fit to the diffractive structure function of (1) for the pseudo-rapidity cut data of [12]. The solid points are experimental data, the solid line represents the E-R model, and the dotted line corresponds to the D-L model. The overall normalization is the sole parameter of each

model, and is determined by a fit to all the data points. The plots shown here correspond to a pomeron intercept of $\alpha_P(0) = 1.08$, corresponding to the soft pomeron intercept of hadron-hadron elastic and diffractive scattering [1]. However, as is discussed further below, we have also obtained similar fits for other choices of the pomeron intercept. From Fig. 5 we can see that the E-R model provides a rather good fit, showing that the harder form factor is an improvement over that used in the D-L model. This point is made in a more quantitative way in Table 3, where the χ^2 for the various fits are given.

Fig. 6a shows the pomeron structure function, F_2^P , of (2), up to the normalization determined above, as a function of Q^2 at fixed β , and Fig. 6b shows the β dependence of F_2^P at fixed Q^2 . Naïvely, one can determine the approximate behaviour of the diffractive structure function as a function of β , at fixed Q^2 and x_P , by looking at the behaviour⁵ of $F_2^{D(3)}$ at small virtuality, k^2 . Then, for example, in the case of the D-L model one would expect to find that

$$F_2^P \sim \beta(1 - \beta). \quad (12)$$

Further, one can show that in the case of large virtuality constraints ($k_{\min}^2 > 1 \text{ GeV}^2$), the form of F_2^P is modified to

$$F_2^P \sim \beta(1 - \beta)^2. \quad (13)$$

However, there is an additional contribution to the β dependence in experiments with a large virtuality constraint, arising from the lower limit of the k^2 phase space integral. We can see from Table 2 that, at fixed Q^2 and x_P , k_{\min}^2 decreases approximately linearly with increasing β . Hence, for the D-L model, in which the form factor introduces an approximately $1/k^4$ dependence into the cross section, we would expect to see a rather strong suppression in the “pomeron structure function” at small β . This is clearly observed in the dotted curve of Fig. 6b.

The harder form factor model of E-R has an approximately $1/k^2$ dependence introduced by the form factor, so such a strong suppression is not expected. Furthermore, this choice of form factor leads to a $\ln(Q^2/\mu^2)$ behaviour in the diffractive cross section, which reflects contributions from the whole range of k^2 , and hence the small k^2 approximation is expected to be relatively poor. In Fig. 6b we see that, even for data with a relatively large rapidity cut, the E-R model predicts a rather flat β distribution of F_2^P , in better agreement with the experimental data. Further, as discussed earlier, as a result of the large pseudo-rapidity gap cuts, we expect a further x_P dependence from the lower limit of the phase-space integral. This means that a “pomeron structure function” defined by multiplying the diffractive structure function by an appropriate power of x_P will not be independent of x_P . Hence, for such data we cannot define a “pomeron structure function”, F_2^P . In order to have a meaningful comparison with F_2^P data, therefore, it is necessary to consider the diffractive structure function at fixed x_P . In the fits shown in Figs. 6, 8 and 10, data are plotted for which $x_P \approx 0.0065$. The model curves are calculated at the corresponding x_P values, and, where there are no data in Q^2 and β with appropriate x_P , the theory points are calculated

⁵In the case that the diffractive structure function factorizes to give a pomeron structure function, this is the dependence of F_2^P at fixed Q^2 .

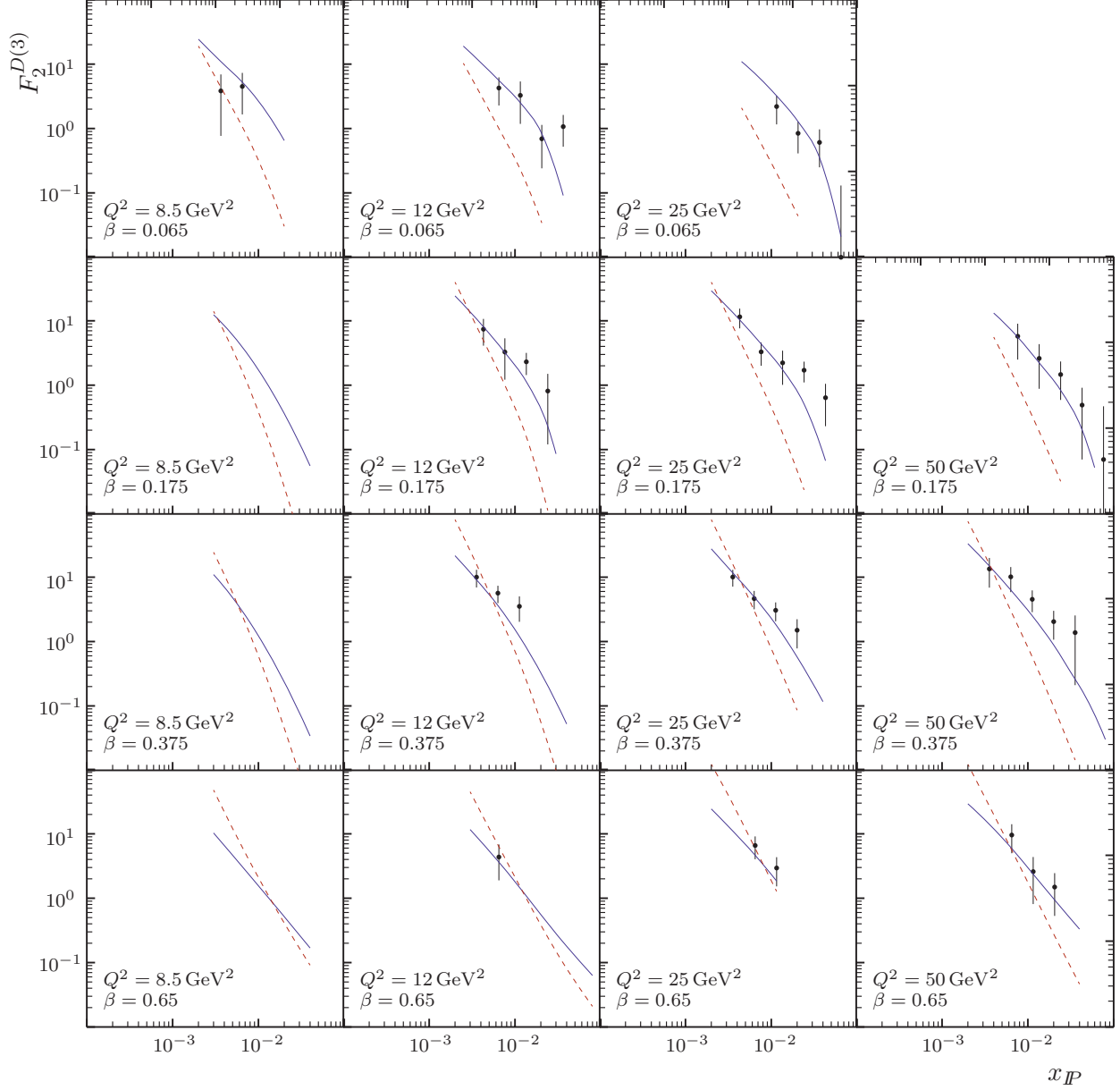


Figure 5: The E-R and D-L form-factor models are fitted to data for $F_2^{D(3)}$ with a virtuality cut. The data sample corresponds to a pseudo-rapidity cut at hadron level of $\eta_{\max} = 1.8$, the pomeron intercept is here assumed to be $\alpha_P(0) = 1.08$, and in the form factors of (10) (D-L) and (11) (E-R) the parameter Λ is chosen to be 0.2 GeV . The points correspond to data from [12] for which $-k_{\min}^2 > 1 \text{ GeV}^2$, and the statistical and systematic errors have been added in quadrature. The solid line is the prediction from the E-R model with the overall normalization determined by a fit to the data points. The dashed line is the D-L model with the same normalization procedure.

using the value $x_P = 0.00649$, which is the most common value of x_P of the plotted data points.

For comparison, we show in Figs. 7 and 8 the equivalent fits for the case of the colour-singlet part of single-gluon exchange (solid line) and the pomeron-quark coupling contribution to the scalar pomeron model (dotted line).

In Figs. 9 and 10 we show the fits using the two-gluon exchange model of Diehl [11]. The most striking feature here is the failure of the model to describe the small- β dependence of the pseudo-rapidity cut data. The reason for this may be seen in the analytic form presented by equation (30) of [11], which shows that, for large $p_{\perp \min}^2$, there is a β^3 dependence, in disagreement with the rather flat dependence found experimentally. Only if the $p_{\perp \min}^2$ cut is removed does the two-gluon term generate an approximately linear β dependence.

We have also considered the diffractive scattering models for the case of a larger pomeron intercept, $\alpha_P(0) = 1.2$, which corresponds to the pomeron intercept favoured in recent H1 and ZEUS analyses [8, 20]. This choice of intercept does not provide a significantly different fit, as can be seen in Table 3. This indicates that the present data are not sufficiently precise to determine the intercept accurately. As may be seen from Table 3, the fits are also reasonable for the choice $\alpha_P(0) = 1$. This corresponds to the use of the x_P dependence as given by the graphs themselves, a procedure adopted in [13, 16].

	χ^2/dof		
	$\alpha_P(0) = 1.08$	$\alpha_P(0) = 1.2$	$\alpha_P(0) = 1$
E-R: $f(k^2) = \sqrt{\frac{\Lambda^2}{\Lambda^2 - k^2}}$	37/41	54/41	30/41
D-L: $f(k^2) = \frac{\Lambda^2}{\Lambda^2 - k^2}$	102/41	97/41	179/41
Single gluon:	64/41	57/41	69/41
Two gluon (Diehl):	137/41	136/41	137/41
Scalar (VBLV):	48/41	61/41	40/41

Table 3: *Results of the fits of various colour-singlet exchange models to the $F_2^{D(3)}$ structure function data from [12].*

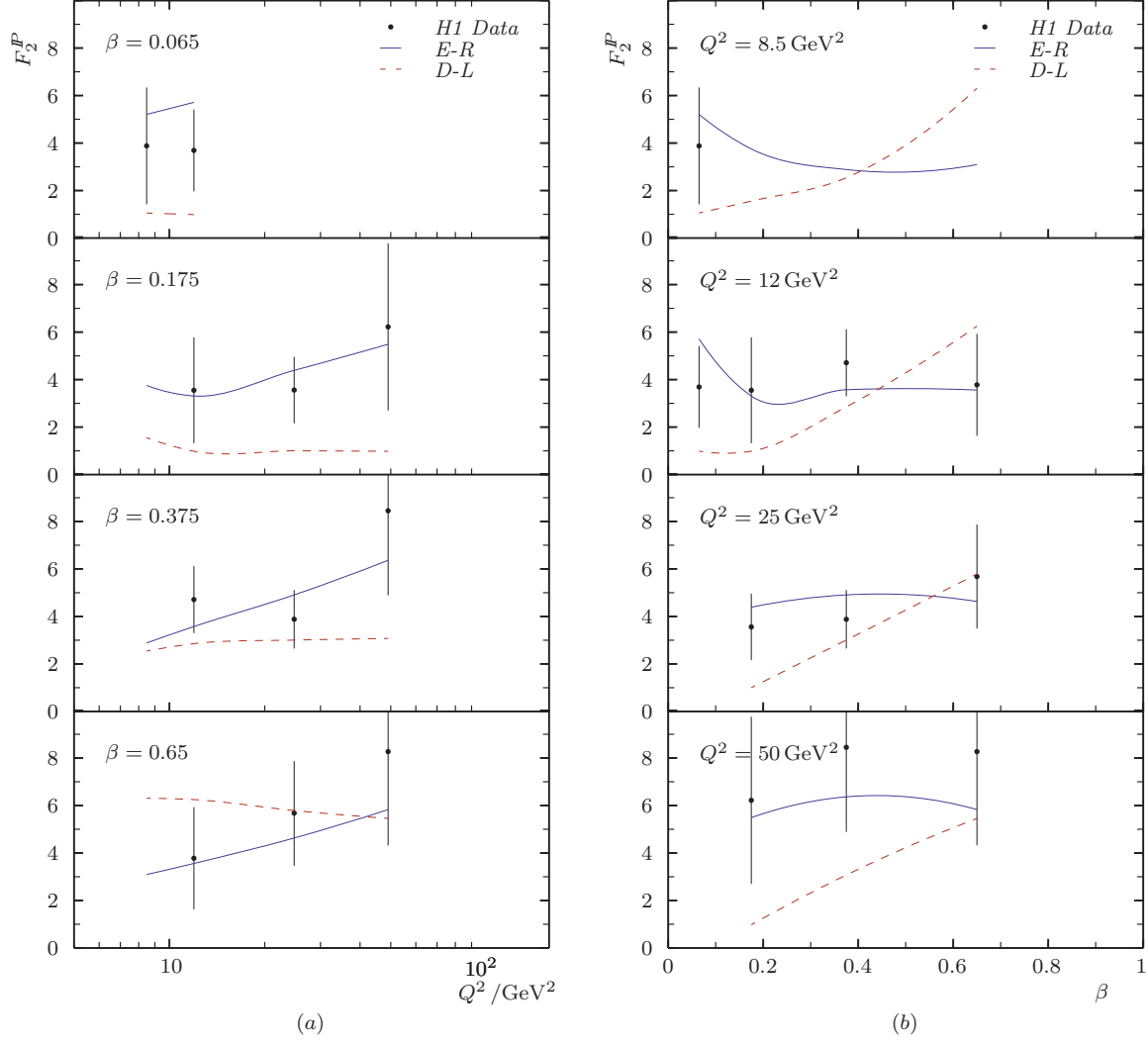


Figure 6: The E-R and D-L form factor models are fitted to the virtuality cut data [12] for the structure function F_2^P , with parameters as in Fig. 5. The solid line is the prediction from the E-R model as determined in Fig. 5, and the dashed line is the D-L model.

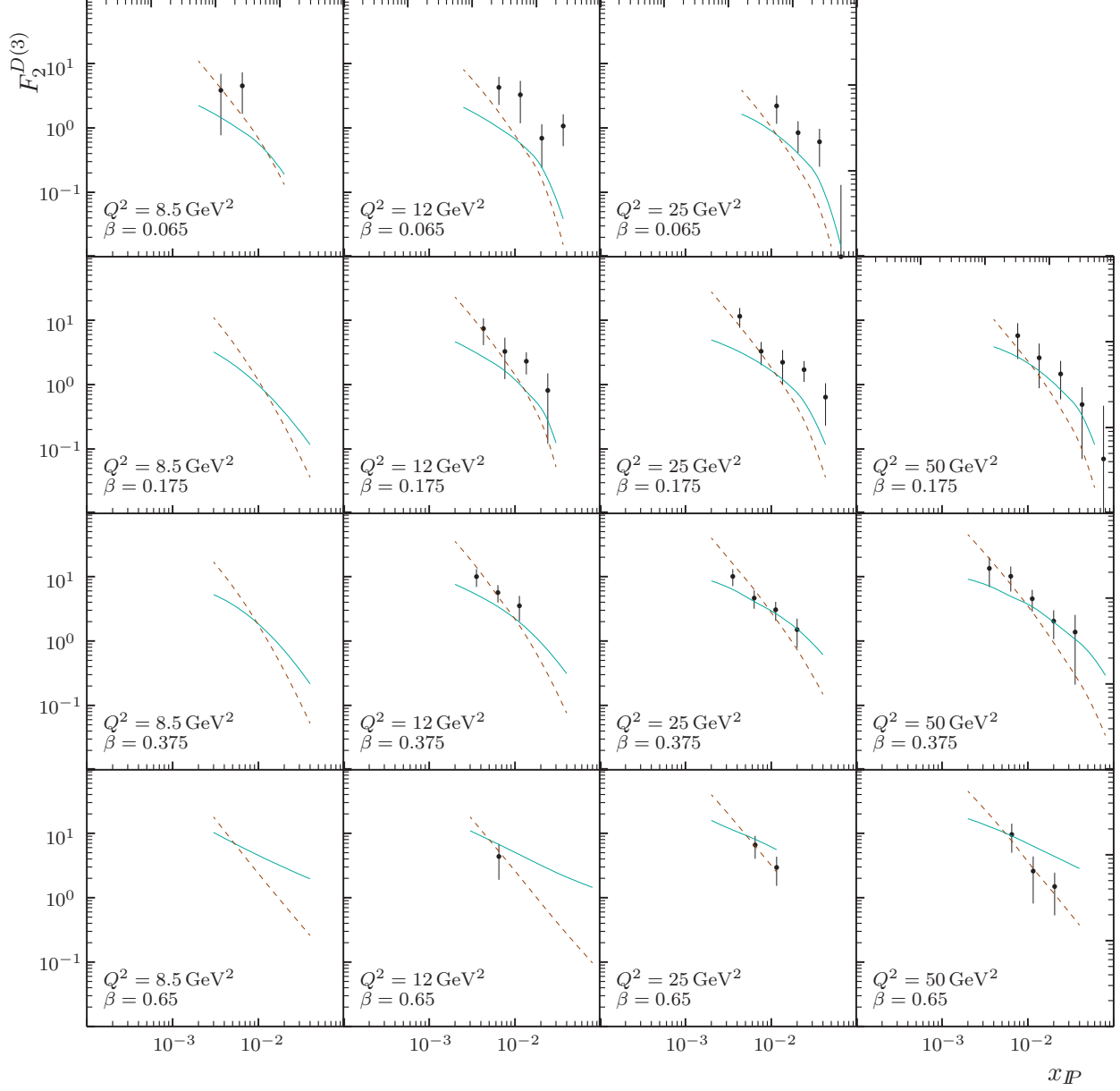


Figure 7: The single-gluon exchange and scalar-pomeron models are fitted to virtuality-cut data [12] for $F_2^{D(3)}$, with parameters as in Fig. 5. The solid line is the prediction from the single-gluon exchange model, and the dashed line is the scalar pomeron model.

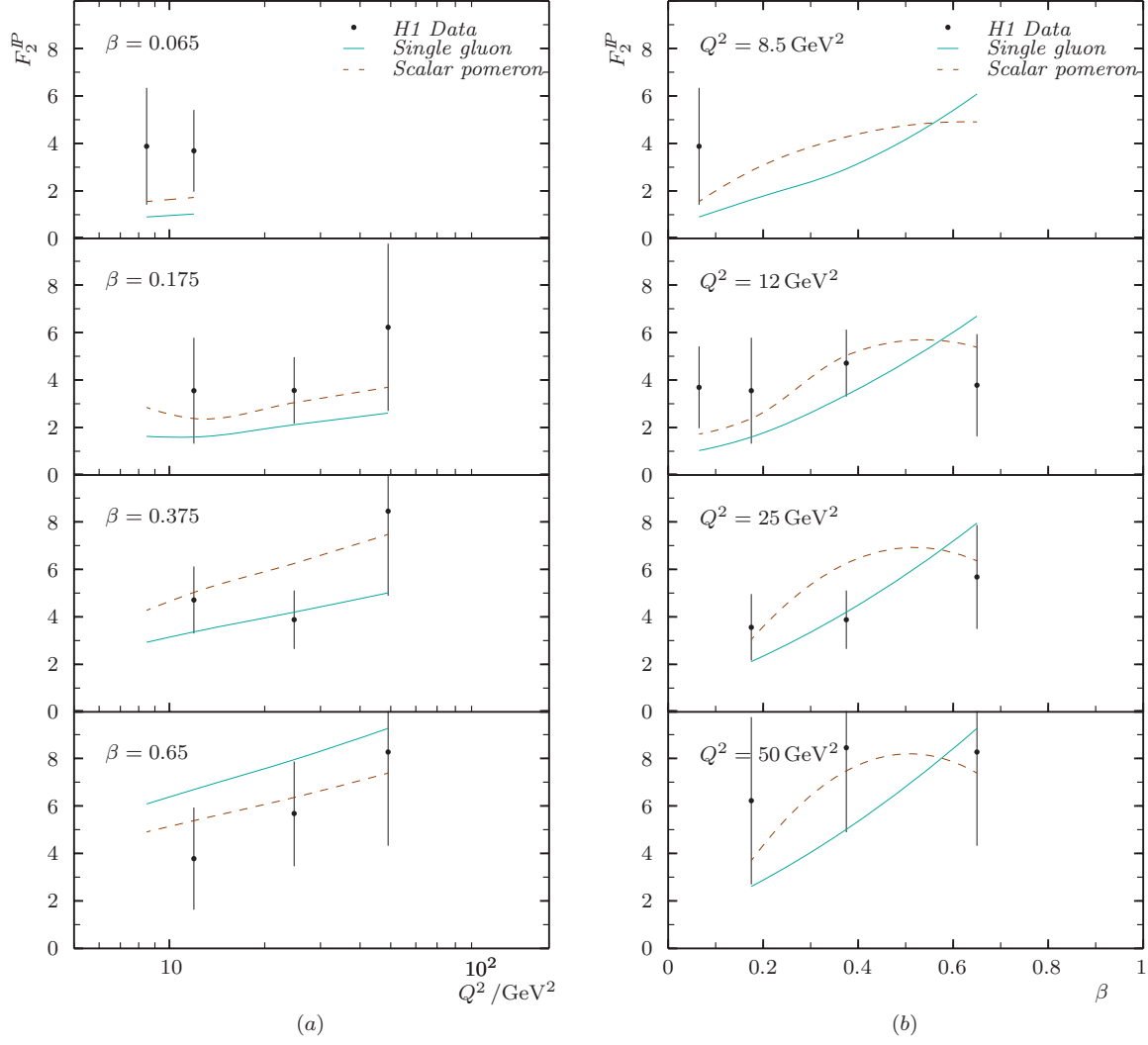


Figure 8: The single-gluon exchange and scalar-pomeron models are fitted to virtuality cut data [12] for F_2^P , with parameters as in Fig. 5. The solid line is the prediction from the single-gluon exchange model, and the dashed line is the scalar pomeron model.

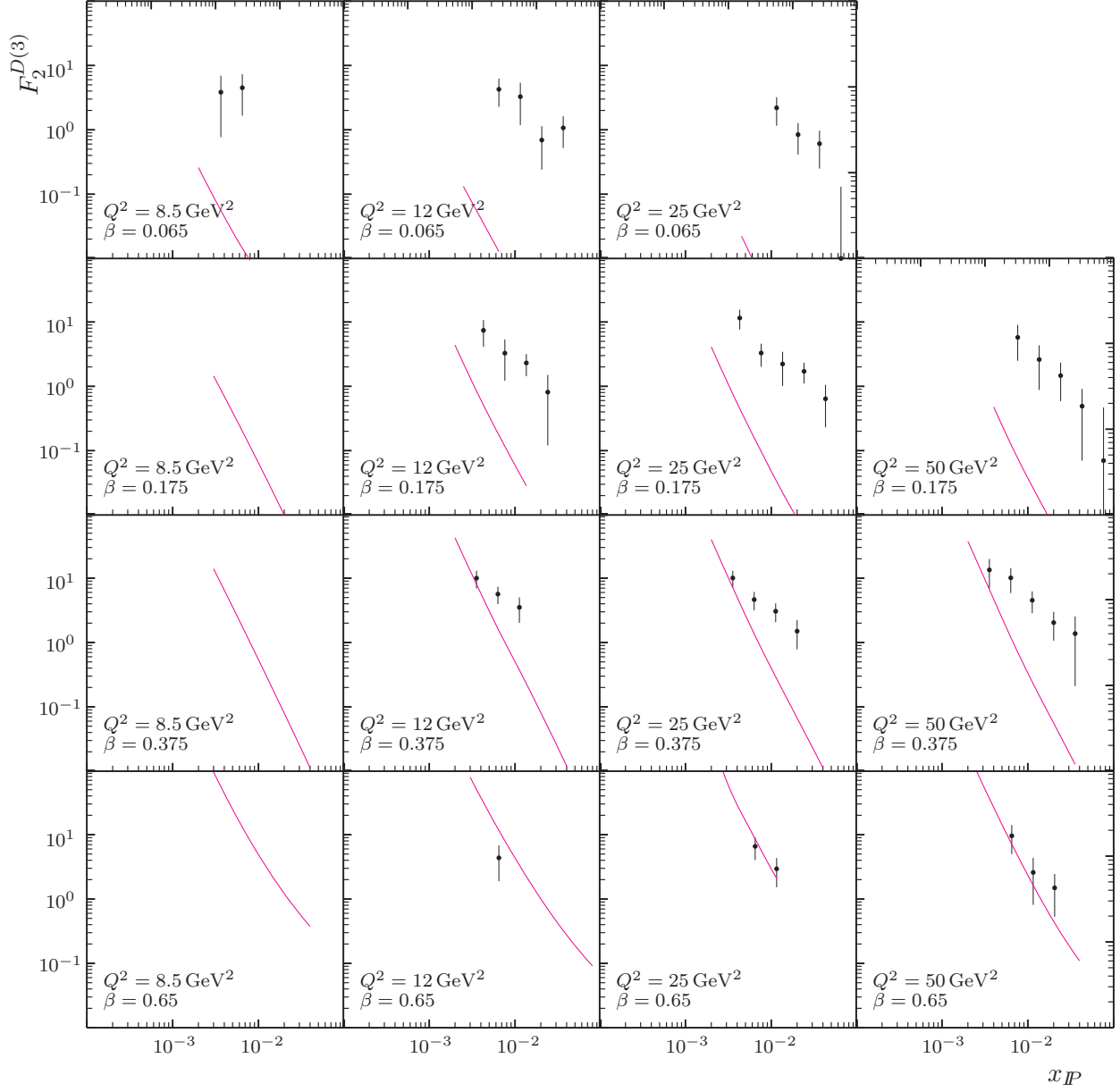


Figure 9: The two-gluon exchange model is fitted to virtuality cut data [12] for $F_2^{D(3)}$, with parameters as in Fig. 5.

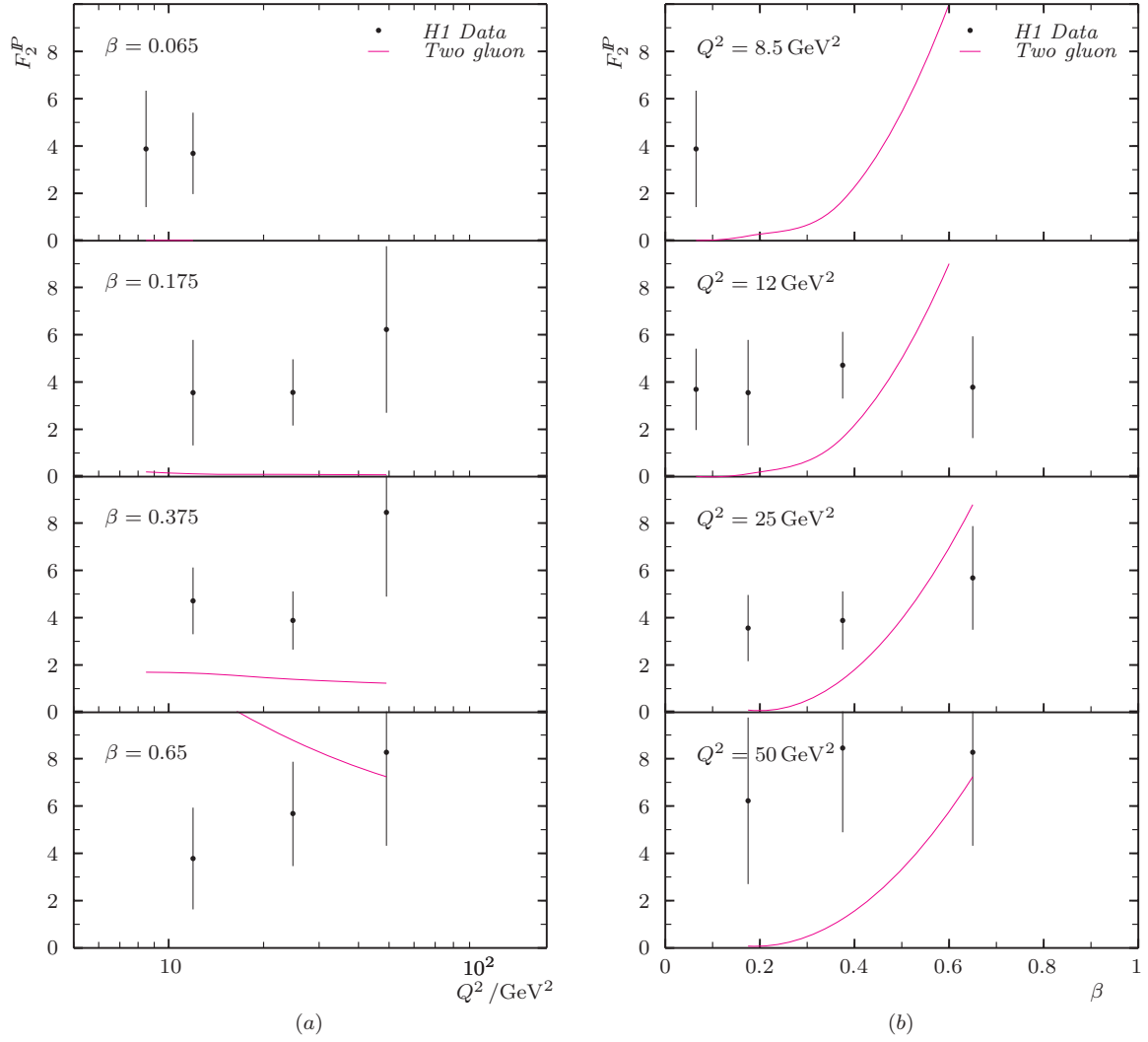


Figure 10: The two-gluon exchange model is fitted to virtuality cut data [12] for F_2^P , with parameters as in Fig. 5.

6 Future Experiments

As has been discussed previously [7] and was also discussed above, H1 and ZEUS analyses in which only events with very large pseudo-rapidity gaps were selected are not described by the resolved-coupling picture as previously formulated [4], as the cuts force the partons coupling to the pomeron to have large virtualities. Thus these experiments provide a very strong test of models of the colourless component of the pomeron coupling to the virtual quark. Here we wish to stress that these tests can be made more stringent by relatively straightforward measurements.

For a given pseudo-rapidity cut, one can calculate the region of parameter space in Q^2 , β and x_P in which one would expect to see strong virtuality constraints due to the cut, using the results presented in Appendices A.1 and A.2. There are a number of ways one can use this information to test these ideas. The dependence of the exchanged parton virtuality on pseudo-rapidity cuts and kinematic parameters could best be studied by examining two samples of data. The first should be chosen with a relatively strong pseudo-rapidity cut, in a region where the cuts force $|k^2| \gtrsim$ a few GeV^2 . The second set should be chosen to differ from the first only in the strength of the pseudo-rapidity cut. For a stronger cut, one would expect to see a relative reduction in the extracted diffractive structure function due to there being less phase space available for the scattering interaction. This is a model-independent effect, and does not require knowledge of the overall normalization.

The size of the reduction is a direct indication of the magnitude of the colourless component of the pomeron coupling to the virtual quark system. The magnitude of this reduction is predicted differently by the various models of diffractive scattering, and hence offers a sensitive way to discriminate between them. At present, we know of only one such study with data chosen with two different pseudo-rapidity cuts [8], but the virtuality constraints used are insufficient to provide a significant reduction in phase space.

Finally, as noted above, the Q^2 , β and x_P dependence of the pseudo-rapidity cut provides a further sensitive test of the models. At present, the data available for such a study [12] have rather poor statistics, but can already discriminate between several of the models presented here. More accurate data would be extremely useful in refining the selection between models.

7 Summary and Conclusions

In this paper we have re-examined the information that can be obtained from the pseudo-rapidity gap dependence of diffractive deep-inelastic scattering. The main conclusion, up to graphs involving soft parton emission, is that a strong pseudo-rapidity cut requires that the resolved partonic component of the Pomeron must be colourless, i.e., the coupling of the Pomeron for partonic states of high virtuality or the coupling is via colour-singlet states. This may be achieved either by postulating a direct coupling with an associated form factor or by modelling it via multi-gluon and multi-quark states. Imposing the pseudo-rapidity cut provides a way to measure this component in the coupling of the Pomeron.

Analysis of the available data with strong pseudo-rapidity cuts shows that the cross section is relatively insensitive to the cut, implying that the direct or multi-parton component

of the pomeron coupling makes a significant contribution. The fit assuming a direct $C = +1$ vector-like coupling to quarks is sensitive to the form factor describing the dependence on the virtuality of the quark. An excellent fit is obtained using the hard E-R form factor, whereas the softer D-L form is not consistent with the data. A good fit is also obtained for the scalar pomeron case. A marginally acceptable fit is also obtained for the case that diffractive scattering is described by the leading-twist single-gluon component with colour dressing due to soft gluons. This contribution necessarily has the pomeron momentum carried by the single gluon. If this is indeed the source of the large pseudo-rapidity gap events, the fact that these events are a sizeable part of the full diffractive deep-inelastic events implies that a significant partonic component of the Pomeron has all of its momentum carried by a single gluon.

This is very interesting in terms of the recent H1 fit of diffractive structure function data [8] using the diagrams of Figs. 1 and 2, which favoured a strongly peaked gluon component with one very hard gluon. However, the H1 calculation considered only the resolved-coupling component of the pomeron, which we argue here is unable to describe data for which the pseudo-rapidity cut imposes strong virtuality constraints. Further, it was suggested in [7] that the contribution from Fig. 3 might have significant scaling violations which, if included in the H1 fit, might enable a less extreme pomeron structure to be fitted to the observed diffractive structure function scaling violations. We also note that there are alternative fits to the H1 data in a two-gluon exchange model [19].

Perhaps the most significant feature of the comparison of the models with data is the failure of the two-gluon model of Diehl to fit the observed β dependence. The reason for this is that, with a large pseudo-rapidity gap cut, there is a strong bound on the lowest p_{\perp}^2 available. Imposing this, the model predicts a β^3 dependence for the structure function, which is in strong disagreement with experiment. One may ask whether this feature persists in all two-gluon exchange models, as Diehl assumes a particular form for the “non-perturbative” gluon propagators. In the case of the more phenomenological model of [19] it is easy to check that the β^3 behaviour should also apply to the $q\bar{q}$ longitudinal and transverse components. The only remaining term in the model which might give a better β dependence for the case of a strong p_{\perp}^2 lower bound is the $q\bar{q}g$ component. Unfortunately we do not know this dependence at present.

Given the sensitivity of various models of diffractive processes in deep-inelastic scattering to the pseudo-rapidity cut, it would be of great interest to obtain improved statistics for such processes. This may allow us to distinguish between the direct coupling and the leading-twist models.

Acknowledgments

J.W. wishes to thank Julian Phillips for helpful discussions and to gratefully acknowledge funding by a Commonwealth Scholarship.

Appendix A

A.1 Constraints on Parton Virtualities in Dijet Production

Here we consider the effect of pseudo-rapidity cuts on the virtuality of the exchanged quark in Fig. 1. This calculation was originally reported in [7], which also includes an analysis of the data shown in Table 1. In this Appendix we present the derivation of this result. The outline is as follows: we start with pseudo-rapidity defined in terms of the polar angle in the laboratory (LAB) frame, and then boost to the photon-pomeron centre-of-mass (CMS) frame, which is also the CMS frame of the hadronic jets in the diffractively-produced system X . From this one can relate pseudo-rapidity to struck quark virtuality in terms of the kinematic invariants, and therefore determine the minimum virtualities, k_{\min}^2 , implied by the pseudo-rapidity cuts, η_{\max} , for each set of parameters, β , Q^2 , and x_P .

We consider diffractive $e - P$ deep-inelastic scattering via dijet production in the HERA LAB frame:

$$e(p_e) + P(P) \rightarrow e(p'_e) + X(X_{\text{lab}}) + P(P'), \quad (\text{A.1})$$

where the momenta of the particles are shown in brackets, and M_X^2 is the invariant mass squared of the diffractive system X composed of the two outgoing jets, as shown in Fig. 11. In the LAB frame,

$$\begin{aligned} p_e &= (E_e, 0, 0, -E_e) & E_e &= 27.5 \text{ GeV} \\ P &= (E_P, 0, 0, E_P) & E_P &= 820 \text{ GeV} \\ p'_e &= (E'_e, E'_e \sin \theta_{\text{lab}}, 0, E'_e \cos \theta_{\text{lab}}) \\ q &= (E_e - E'_e, -E'_e \sin \theta_{\text{lab}}, 0, -E_e - E'_e \cos \theta_{\text{lab}}), \end{aligned} \quad (\text{A.2})$$

and we parameterize the lower quark momentum generally by

$$p_B = (l, l \sin \theta'_{\text{lab}} \cos \phi_{\text{lab}}, l \sin \theta'_{\text{lab}} \sin \phi_{\text{lab}}, l \cos \theta'_{\text{lab}}). \quad (\text{A.3})$$

Here we have assumed that the pomeron is emitted in the proton direction and carries a fraction x_P of the proton initial momentum.

The following relations are useful:

$$Q^2 = -q^2 = -(p_e - p'_e)^2 = 2p_e \cdot p'_e = 2E_e E'_e (1 + \cos \theta_{\text{lab}}) \quad (\text{A.4})$$

and

$$\begin{aligned} W^2 = (P + q)^2 \Rightarrow W^2 + Q^2 = 2P \cdot q &= 2E_P(E_e - E'_e + E_e + E'_e \cos \theta_{\text{lab}}) \\ &= 2E_P[2E_e - E'_e(1 - \cos \theta_{\text{lab}})]. \end{aligned} \quad (\text{A.5})$$

Hence

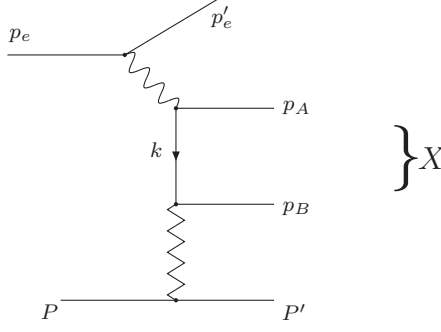


Figure 11: *Momentum assignments for dijet production.*

$$E'_e(1 + \cos \theta_{\text{lab}}) = \frac{Q^2}{2E_e} \quad (\text{A.6})$$

$$E'_e(1 - \cos \theta_{\text{lab}}) = 2E_e - \frac{Q^2 + W^2}{2E_P}. \quad (\text{A.7})$$

Therefore, adding (A.6) and (A.7), we get

$$2E'_e = 2E_e + \frac{Q^2}{2E_e} - \frac{Q^2}{2E_P\beta x_P}, \quad (\text{A.8})$$

and, subtracting,

$$2E'_e \cos \theta_{\text{lab}} = -2E_e + \frac{Q^2}{2E_e} + \frac{Q^2}{2E_P\beta x_P}. \quad (\text{A.9})$$

We can therefore write the momentum of the diffractive system as

$$\begin{aligned} X_{\text{lab}} &= (x_P E_P + E_e - E'_e, -E'_e \sin \theta_{\text{lab}}, 0, x_P E_P - E_e - E'_e \cos \theta_{\text{lab}}), \\ &= \left(x_P E_P + \frac{Q^2}{2} \left[\frac{1}{2E_P\beta x_P} - \frac{1}{2E_e} \right], - \left[Q^2 \left(1 - \frac{Q^2}{2E_P E_e \beta x_P} \right) \right]^{\frac{1}{2}}, \right. \\ &\quad \left. 0, x_P E_P - \frac{Q^2}{2} \left[\frac{1}{2E_P\beta x_P} + \frac{1}{2E_e} \right] \right). \end{aligned} \quad (\text{A.10})$$

In the CMS frame, the momentum of the diffractive system is

$$X_{\text{cms}} = (M_X, 0, 0, 0). \quad (\text{A.11})$$

We now carry out two Lorentz boosts to get from the LAB frame to the jet-jet CMS frame, seeking to remove the spatial components of X_{lab} . The first boost we take along the z axis, with boost parameter β_1 . The required boost satisfies $X_{\text{lab}}^z - \beta_1 X_{\text{lab}}^0 = 0$, giving

$$\beta_1 = \frac{-\left[\frac{Q^2}{2}\left(\frac{1}{2E_P\beta x_{\mathcal{P}}} + \frac{1}{2E_e}\right) - x_{\mathcal{P}}E_P\right]}{\frac{Q^2}{2}\left(\frac{1}{2E_P\beta x_{\mathcal{P}}} - \frac{1}{2E_e}\right) + x_{\mathcal{P}}E_P}. \quad (\text{A.12})$$

After this first boost, we have

$$\begin{aligned} X_{\text{lab}}^0 \rightarrow X'^0 &= \frac{1}{\sqrt{1-\beta_1^2}} \left[x_{\mathcal{P}}E_P + \frac{Q^2}{2} \left(\frac{1}{2E_P\beta x_{\mathcal{P}}} - \frac{1}{2E_e} \right) - \right. \\ &\quad \left. \beta_1 \left\{ x_{\mathcal{P}}E_P - \frac{Q^2}{2} \left(\frac{1}{2E_P\beta x_{\mathcal{P}}} + \frac{1}{2E_e} \right) \right\} \right] \\ &= \frac{\sqrt{1-\beta_1^2}}{\beta_1} \left[x_{\mathcal{P}}E_P - \frac{Q^2}{2} \left(\frac{1}{2E_P\beta x_{\mathcal{P}}} + \frac{1}{2E_e} \right) \right], \\ X'^x &= X_{\text{lab}}^X. \end{aligned} \quad (\text{A.13})$$

We now boost along the x direction, which requires a boost parameter β_2 satisfying

$$X'^x - \beta_2 X'^0 = 0, \quad (\text{A.14})$$

giving

$$\beta_2 = \frac{\beta_1}{\sqrt{1-\beta_1^2}} \frac{\left[Q^2 \left(1 - \frac{Q^2}{4E_e E_P \beta x_{\mathcal{P}}} \right) \right]^{\frac{1}{2}}}{\frac{Q^2}{2} \left(\frac{1}{2E_P\beta x_{\mathcal{P}}} + \frac{1}{2E_e} \right) - x_{\mathcal{P}}E_P}. \quad (\text{A.15})$$

These two boosts take us to the jet-jet CMS frame.

Now we consider the jet produced by the lower parton line in the LAB frame. Consider the effect of the previous two boosts on the 0th component of p_B :

$$\begin{aligned} \beta_1 : p_B^0 \rightarrow p_B'^0 &= \frac{l}{\sqrt{1-\beta_1^2}} (1 - \beta_1 \cos \theta_{\text{lab}}), \\ \beta_2 : p_B'^0 \rightarrow p_{B\text{cms}}^0 &= \frac{l}{\sqrt{1-\beta_2^2}} \left[\frac{(1 - \beta_1 \cos \theta_{\text{lab}})}{\sqrt{1-\beta_1^2}} - \beta_2 \sin \theta_{\text{lab}} \cos \phi_{\text{lab}} \right]. \end{aligned} \quad (\text{A.16})$$

Remembering that

$$P_{\text{lab}} = (E_P, 0, 0, E_P), \quad (\text{A.17})$$

we see that the effect of the boosts on the 0th component of the proton initial momentum is

$$\begin{aligned}
\beta_1 : \quad P^0 &\rightarrow P'^0 = \frac{(1 - \beta_1)}{\sqrt{1 - \beta_1^2}} E_P = \sqrt{\frac{1 - \beta_1}{1 + \beta_1}} E_P, \\
\beta_2 : \quad P'^0 &\rightarrow P_{\text{cms}}^0 = \sqrt{\frac{1 - \beta_1}{1 + \beta_1}} \frac{E_P}{\sqrt{1 - \beta_2^2}}.
\end{aligned} \tag{A.18}$$

For general on shell 4-vectors p and q , we have

$$p \cdot q = p^0 q^0 (1 - \cos \theta), \tag{A.19}$$

where θ is the angle between p and q . So we have

$$\begin{aligned}
P \cdot p_B &= P^0 p_B^0 (1 - \cos \theta_{\text{lab}}) \\
&= P_{\text{cms}}^0 p_{B \text{ cms}}^0 (1 - \cos \theta_{\text{cms}}),
\end{aligned} \tag{A.20}$$

where θ_{cms} is the angle of the quark relative to the forward proton direction in the CMS frame, and θ_{lab} is the angle of the quark relative to the forward proton direction in the LAB frame. Hence

$$(1 - \cos \theta_{\text{cms}}) = \frac{(1 + \beta_1)(1 - \beta_2^2)(1 - \cos \theta_{\text{lab}})}{1 - \beta_1 \cos \theta_{\text{lab}} - \sqrt{1 - \beta_1^2} \beta_2 \sin \theta_{\text{lab}} \cos \phi_{\text{lab}}}. \tag{A.21}$$

Thence the constraint follows: a cut on pseudo-rapidity, η_{max} , is equivalent to a cut on the lab angle, $\theta_{\text{lab}}^{\text{min}}$, where

$$\eta = -\ln \tan \frac{\theta_{\text{lab}}}{2} \Rightarrow \cos \theta_{\text{lab}}^{\text{min}} = \frac{1 - e^{-2\eta_{\text{max}}}}{1 + e^{-2\eta_{\text{max}}}}. \tag{A.22}$$

Thus

$$(1 - \cos \theta_{\text{cms}}^{\text{min}}) = \frac{(1 + \beta_1)(1 - \beta_2^2) \frac{2e^{-2\eta_{\text{max}}}}{1 + e^{-2\eta_{\text{max}}}}}{1 - \beta_1 \frac{1 - e^{-2\eta_{\text{max}}}}{1 + e^{-2\eta_{\text{max}}}} - \sqrt{1 - \beta_1^2} \beta_2 \frac{2e^{-\eta_{\text{max}}}}{1 + e^{-2\eta_{\text{max}}}} \cos \phi_{\text{lab}}}, \tag{A.23}$$

from which it follows from (9) that a cut in pseudo-rapidity, η_{max} , corresponds to a minimum virtuality, k_{min}^2 , of the exchanged quark:

$$-k_{\text{min}}^2 = \frac{Q^2}{2\beta} \frac{(1 + \beta_1)(1 - \beta_2^2) \frac{2e^{-2\eta_{\text{max}}}}{1 + e^{-2\eta_{\text{max}}}}}{1 - \beta_1 \frac{1 - e^{-2\eta_{\text{max}}}}{1 + e^{-2\eta_{\text{max}}}} - \sqrt{1 - \beta_1^2} \beta_2 \frac{2e^{-\eta_{\text{max}}}}{1 + e^{-2\eta_{\text{max}}}} \cos \phi_{\text{lab}}}. \tag{A.24}$$

Since we do not know the azimuthal angle ϕ_{lab} , we choose ϕ_{lab} to minimize $|k_{\text{min}}^2|$, and still find that for a large range of parameter space k_{min}^2 is constrained to be much larger than 1 GeV^2 , as seen in Tables 1 and 2.

This calculation demonstrates clearly that dijet production cannot contribute to large pseudo-rapidity gap diffractive DIS for a wide range of the parameters β , Q^2 and x_P .

A.2 Constraints on Parton Virtualities for Production of Three or More Jets

For production of three or more jets, e.g., the processes of Fig. 2, the situation is slightly more complicated. However, here one also finds strong virtuality constraints. It is easiest to consider multi-jet production diffractive processes in the form

$$e(p_e) + P(P) \rightarrow e(p'_e) + X_1(p_A) + X_2(p_B) + P(P'), \quad (\text{A.25})$$

where $X = X_1 + X_2$ is the diffractive system. The system X_2 is the hadronic jet produced by the final-state parton coupled to the pomeron in a diagram such as Fig. 2, and has squared mass $M_{X_2}^2 \lesssim 1 \text{ GeV}^2$. The sum over the jets formed from the other final-state partons in the process is X_1 , and has squared mass $M^2 < M_X^2$. In the example of three-jet production via boson-gluon fusion shown in Fig. 2b, X_1 corresponds to the two upper final-state quark jets, whilst X_2 represents the on-shell emitted gluon. In this diagram, we are looking at constraints on the squared four-momentum of the exchanged gluon.

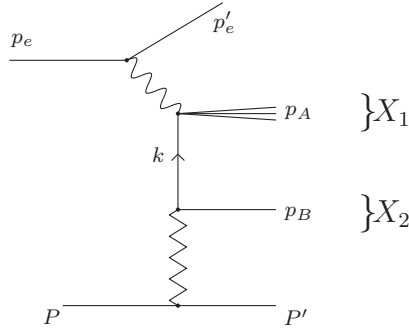


Figure 12: *Momentum assignments for multi-jet production.*

In the CMS frame, we parameterize the jet momenta by

$$\begin{aligned} p_A &= \gamma \frac{M_X^2}{2} \left(\frac{2-\gamma}{\gamma}, -\sin \theta_{\text{cms}}, 0, -\cos \theta_{\text{cms}} \right) \\ p_B &= \gamma \frac{M_X^2}{2} (1, \sin \theta_{\text{cms}}, 0, \cos \theta_{\text{cms}}), \end{aligned} \quad (\text{A.26})$$

where the mass squared of system X_1 is $(1-\gamma)M_X^2$, and $0 < \gamma \leq 1$. The case $\gamma = 1$ corresponds to dijet production. The pomeron momentum in this frame is

$$P_P = (E, 0, 0, E), \quad (\text{A.27})$$

where

$$E = \frac{Q^2 + M_X^2}{2M_X}. \quad (\text{A.28})$$

The momentum of the exchanged parton is given by

$$k = p_A - q = P_P - p_B \quad (\text{A.29})$$

and therefore the virtuality of the exchanged parton is

$$k^2 = -\gamma \frac{Q^2 + M_X^2}{2} (1 - \cos \theta_{\text{cms}}). \quad (\text{A.30})$$

We see that the constraint from the η_{max} cuts, derived in Appendix A.1, can in theory be evaded by having γ small.

Let us first consider the case $\theta_{\text{cms}} > 90^\circ$, in which case the condition that the virtuality of the parton be low (say $\leq 1 \text{ GeV}^2$) requires

$$\gamma \leq 1 \text{ GeV}^2 \cdot \frac{2}{Q^2 + M_X^2} = \frac{2}{k_{\text{max}}^2 (\text{GeV}^2)}. \quad (\text{A.31})$$

From Table 2, we see that for the case that the pseudo-rapidity cut imposes a significant constraint on k_{min}^2 , $k_{\text{min}}^2 > 6 \text{ GeV}^2$, say, $\gamma \leq 1/33$. This corresponds effectively to a two-jet configuration, because the soft parton carrying less than $1/33$ of the Pomeron momentum will not be observed as a jet. The other parton is constrained by the pseudo-rapidity cut to carry essentially all of the Pomeron momentum. As discussed in the text, this contribution is included in the model corresponding to leading twist, but not in the models of direct coupling. The non-soft contributions which are genuinely multi-jet processes may be shown to require high virtuality similar to the two-jet bound. To see this, we note that, from (A.30), the pseudo-rapidity cuts give us

$$\begin{aligned} -k_{\gamma < 1}^2 \geq -k_{\text{min}}^2 &= \gamma \frac{Q^2 + M_X^2}{2} (1 - \cos \theta_{\text{cms}}^{\text{min}}) \\ &= -\gamma k_{\gamma=1}^2, \end{aligned} \quad (\text{A.32})$$

where $k_{\gamma=1}^2$ is the minimum virtuality of the exchanged quark in the dijet production diagram of Fig. 1 allowed by the experimental cuts.

The opening angle of a soft jet will clearly be much greater than for a harder jet. We quantify this statement below. The angles discussed here are shown in Fig. 13. In the HERA LAB frame, θ_1 is the angle between the final-state parton which hadronizes to produce the observed jet, and θ_2 is the opening angle of the hadronic jet. Therefore $\theta_1 - \theta_2$ is the angle between the edge of the hadronic jet and the proton direction, in terms of which the pseudo-rapidity gap is defined.

To estimate the opening angle of a soft jet, we assume that a jet produced by a parton of energy E_j has a cone radius of 0.5 to 1 unit of pseudo-rapidity, and an opening angle of θ_2 . Boosting to a frame in which the parton has energy γE_j , we can find the opening angle, θ'_2 , of the corresponding jet in terms of θ_2 . This is the relation between angles that we shall assume for a soft jet in the HERA LAB frame. Starting with a massless parton with energy E_j , we then boost to a frame in which it has energy γE_j :

$$(E_j, 0, 0, E_j) \rightarrow \gamma (E_j, 0, 0, E_j) \quad (\text{A.33})$$

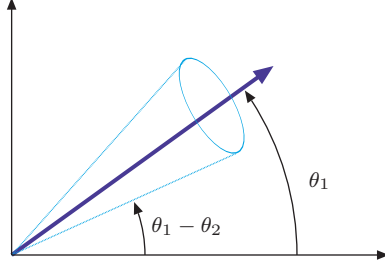


Figure 13: *Pseudo-rapidity definition at the parton and hadron levels.*

If we denote the boost parameters by γ^* and β^* , where $\gamma^* = 1/\sqrt{1 - \beta^{*2}}$, then we have

$$\gamma E_j \rightarrow \gamma^*(E_j - \beta^* E_j) \Rightarrow \gamma = \gamma^*(1 - \beta^*). \quad (\text{A.34})$$

The corresponding transformation of angles is

$$\begin{aligned} \tan \theta'_2 &= \frac{1}{\gamma^*} \frac{\sin \theta_2}{\cos \theta_2 - \beta^*} \\ &= \frac{1}{\gamma^*} \frac{\sin \theta_2 / \cos \theta_2}{1 - \beta^* / \cos \theta_2} \\ &\geq \frac{1}{\gamma^*} \frac{\tan \theta_2}{1 - \beta^*} \\ &= \frac{1}{\gamma} \tan \theta_2 \end{aligned} \quad (\text{A.35})$$

Further, from (A.35), we have

$$\tan \theta'_2 \geq \frac{1}{\gamma} \tan \theta_2 \geq \frac{1}{\gamma} 2 \tan \frac{\theta_2}{2} \quad (\text{A.36})$$

i.e.,

$$\tan \frac{\theta'_2}{2} \geq \frac{1}{\gamma} \tan \frac{\theta_2}{2} (1 - \tan^2 \frac{\theta'_2}{2}) \quad (\text{A.37})$$

To see what sort of bound we can put on $(1 - \tan^2 \frac{\theta'_2}{2})$, we assume that $\theta_1 \leq 90^\circ$, i.e., the jet is produced in the forward hemisphere.

The large pseudo-rapidity cut data from [12] was taken with an experimental cut on pseudo-rapidity of $\eta_{\max} = 1.8$, which corresponds to a minimum angle in the HERA LAB frame with no hadronic activity of $\theta_{\min}^{\text{lab}} \approx 18^\circ$. Therefore

$$\theta'_2 \leq \theta_1 - 18^\circ \Rightarrow 1 - \tan^2 \frac{\theta'_2}{2} \geq 1 - \tan^2 36^\circ \approx 0.47. \quad (\text{A.38})$$

Thus

$$\tan \frac{\theta'_2}{2} \geq \frac{0.47}{\gamma} \tan \frac{\theta_2}{2}. \quad (\text{A.39})$$

Finally, pseudo-rapidity cuts are defined at the experimental level by seeking events with an angle $\theta_1 - \theta_2$ which satisfies the pseudo-rapidity cut η_{\max} :

$$\begin{aligned} \eta_{\max}^{\text{expt}} &\geq -\ln \tan \left(\frac{\theta_1 - \theta_2}{2} \right) \\ &\geq -\ln \left(\tan \frac{\theta_1}{2} - \tan \frac{\theta_2}{2} \right) \\ &= -\ln \tan \frac{\theta_1}{2} - \ln \left(1 - \frac{\tan \frac{\theta_2}{2}}{\tan \frac{\theta_1}{2}} \right) \\ &\Rightarrow -\ln \tan \frac{\theta_1}{2} \leq \eta_{\max}^{\text{expt}} + \ln \left(1 - \frac{\tan \frac{\theta_2}{2}}{\tan \frac{\theta_1}{2}} \right). \end{aligned} \quad (\text{A.40})$$

At the theoretical quark-parton level, we deal with the angle θ_1 , and assume a cone radius of 0.5 to 1 unit of pseudo-rapidity. Therefore

$$-\ln \tan \frac{\theta_1}{2} \leq \eta_{\max}^{\text{th}} \approx \eta_{\max}^{\text{expt}} - \left(\frac{1}{2} \rightarrow 1 \right), \quad (\text{A.41})$$

giving

$$\tan \frac{\theta_2}{2} = {}^{(0.39)}_{(0.63)} \tan \frac{\theta_1}{2}, \quad (\text{A.42})$$

where the factor 0.39 is for the case where one assumes a cone radius of $\frac{1}{2}$, and the lower number is for unit radius.

Putting this all together, we can determine the bound on multi-jet production in terms of the dijet limit calculated in Appendix A.1. Using (A.21), we can write

$$(1 - \cos \theta^{\text{cms}}) = f(1 - \cos \theta^{\text{lab}}), \quad (\text{A.43})$$

where f is a complicated function of the LAB angles and boost parameters. We therefore have:

$$\begin{aligned} k_{\gamma < 1}^2 &= \gamma \frac{Q^2 + M_X^2}{2} (1 - \cos \theta_1^{\text{cms}}) \\ &= \gamma \frac{Q^2 + M_X^2}{2} f(1 - \cos \theta_1^{\text{lab}}) \\ &= \gamma \frac{Q^2 + M_X^2}{2} f \tan \frac{\theta_1^{\text{lab}}}{2} \sin \theta_1^{\text{lab}} \end{aligned}$$

$$\begin{aligned}
&\geq \gamma \frac{Q^2 + M_X^2}{2} f \tan \frac{\theta_2'^{\text{lab}}}{2} \sin \theta_1^{\text{lab}} \\
&\geq 0.47 \frac{Q^2 + M_X^2}{2} f \tan \frac{\theta_2^{\text{lab}}}{2} \sin \theta_1^{\text{lab}} \\
&= 0.47 \frac{Q^2 + M_X^2}{2} f_{(0.39)} \tan \frac{\theta_1^{\text{lab}}}{2} \sin \theta_1^{\text{lab}} \\
&\approx_{(0.3)}^{(0.2)} \frac{Q^2 + M_X^2}{2} f \tan \frac{\theta_1^{\text{lab}}}{2} \sin \theta_1^{\text{lab}} \\
&=_{(0.3)}^{(0.2)} \frac{Q^2 + M_X^2}{2} f (1 - \cos \theta_1^{\text{lab}}) \\
&=_{(0.3)}^{(0.2)} \frac{Q^2 + M_X^2}{2} (1 - \cos \theta_1^{\text{cms}})
\end{aligned} \tag{A.44}$$

i.e.

$$k_{\gamma < 1}^2 \gtrsim_{(0.3)}^{(0.2)} k_{\gamma = 1}^2 \tag{A.45}$$

Thus, considering this result along with the dijet virtuality limits shown in Table 2, we see that for all jet production, $0 < \gamma \leq 1$, for a large region of parameter space, resolved jet production by diagrams such as those shown in Figs. 1 and 2 does not contribute to the large pseudo-rapidity gap sample.

A.3 Multi-Jet Production – Special Case

We now consider a scenario which is not covered by either of the cases described above. This is where the lower parton coupled to the pomeron emits a gluon, or there is some other QCD radiation, after it interacts with the pomeron.

We consider the case of dijet production, noting that the discussion for multi-jet production proceeds in an analogous way, with the modification that the lower quark coupled to the pomeron emits final state radiation by single gluon emission. This process is shown in Fig. 14.

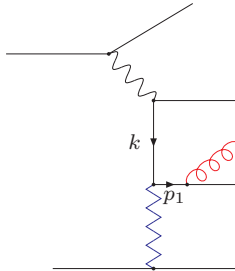


Figure 14: *Gluon bremsstrahlung in pomeron exchange.*

In a resolved-coupling picture, the quark labelled p_1 should be close to mass shell. In this case, the quark momentum at the lower vertex, p_1 , is shared between the two final-state partons, which, following our argument in Appendix A.2, means that the jets from the hadronization of these partons will be more spread than the jet from one final-state parton carrying all the momentum. The jets from the final-state partons are all constrained by the pseudo-rapidity cuts to be separated from the pomeron direction by a minimum angle θ_{\min} , and, since they will spread more than a harder jet, the angle between the hadronizing partons will be wider and hence the constraint in this case is stronger than that for a single hard parton at the lower vertex.

It should be clear from the discussion we present here that the case for single-gluon bremsstrahlung is sufficient to illustrate the case for emission of higher numbers of partons from the lower line.

References

- [1] A. Donnachie and P. V. Landshoff, Nucl. Phys. **B231**, 189 (1984); Nucl. Phys. **B244**, 322 (1984); Nucl. Phys. **B267**, 690 (1986); Phys. Lett. **B296**, 227 (1992)
- [2] H1 Collaboration, T. Ahmed *et al.*, Nucl. Phys. **B429**, 477 (1994); Nucl. Phys. **B435**, 3 (1995); ZEUS Collaboration, M. Derrick *et al.*, Phys. Lett. **B315**, 481 (1993)
- [3] ZEUS Collaboration, M. Derrick *et al.*, Phys. Lett. **B332**, 228 (1994)
- [4] G. Ingelman and P. E. Schlein, Phys. Lett. **152B**, 256 (1985)
- [5] H1 Collaboration, T. Ahmed *et al.*, Phys. Lett. **B348**, 681 (1995)
- [6] ZEUS Collaboration, J. Breitweg *et al.*, Eur. Phys. J. **C1**, 81 (1998)
- [7] J. Ellis and G. G. Ross, Phys. Lett. **B384**, 293 (1996)
- [8] H1 Collaboration, C. Adloff *et al.*, Z. Phys. **C76**, 613 (1997)
- [9] A. Donnachie and P. V. Landshoff, Phys. Lett. **185B**, 403 (1987); Phys. Lett. **191B**, 309 (1987)
- [10] J. Vermaseren, F. Barreiro, L. Labarga, and F. J. Yndurain, Phys. Lett. **B418**, 363 (1998)
- [11] M. Diehl, Z. Phys. **C66**, 181 (1995)
- [12] J. P. Phillips, Ph.D. thesis, University of Manchester, 1995, available from <http://www-h1.desy.de/h1/www/h1work/dif/publications.html>
- [13] F. Hautmann, Z. Kunszt and D. E. Soper, Phys. Rev. Lett. **81**, 3333 (1998)
- [14] J. C. Collins, Phys. Rev. **D57**, 3051 (1998)

- [15] M. Genovese, N. N. Nikolaev, and B. G. Zakharov, J. Exp. Theor. Phys. **81**, 625 (1995); Phys. Lett. **B380**, 213 (1996); J. Bartels, C. Ewerz, H. Lotter, M. Wüsthoff, and M. Diehl, hep-ph/9609239; J. Bartels, H. Lotter, and M. Wüsthoff, Phys. Lett. **B379**, 239 (1996); A. Bialas and R. Peschanski, Phys. Lett. **B378**, 302 (1996); Phys. Lett. **B387**, 405 (1996); E. Gotsman, E. Levin, and U. Maor, Nucl. Phys. **B493**, 354 (1997)
- [16] N. Nikolaev and B. G. Zakharov, Z. Phys. **C53**, 331 (1992)
- [17] M. Diehl, hep-ph/9803296
- [18] W. Buchmüller and A. Hebecker, Phys. Lett. **B355**, 573 (1995)
- [19] J. Bartels, J. Ellis, H. Kowalski and M. Wüsthoff, hep-ph/9803497
- [20] ZEUS Collaboration, J. Breitweg *et al.*, Eur. Phys. J. **C6**, 43 (1999)